American Journal of Pathology, Vol. 167, No. 4, October 2005

Cardiovascular, Pulmonary and Renal Pathology

Analysis of Tumor Vessel Supply in Lewis Lung Carcinoma in Mice by Fluorescent Microsphere Distribution and Imaging with Micro- and Flat-Panel Computed Tomography

Rajkumar Savai,* Joachim C. Wolf,† Susanne Greschus,‡ Bastian G. Eul,* Ralph T. Schermuly,* Jörg Hänze,* Robert Voswinckel,* Alexander C. Langheinrich,† Friedrich Grimminger,* Horst Traupe,‡ Werner Seeger,* and Frank Rose*

From the Departments of Internal Medicine/Pulmonary and Critical Care Medicine, Radiology,† and Neuroradiology,‡ Justus Liebig University, Giessen, Germany*

In lung carcinomas the blood supply varies depending on tumor type and stage and can develop from pulmonary or bronchial circulation, or both. To examine this *in vivo*, primary bronchogenic Lewis lung carcinoma cells were intratracheally instilled in C57BL/6 mice. Within 7 days, histological examinations showed progressive tumor growth at the peripheral parenchymal region. The relative contribution of tumor blood supply via the pulmonary and systemic arteries was studied in detail using fluorescent microspheres (10 μm). When compared to healthy lung parenchyma (13:1), Lewis lung carcinoma tumor tissue (52:1) showed a fourfold increase in pulmonary to systemic microspheres, indicating that the pulmonary arteries are the predominant tumor-feeding vessels. After filling the vessels with a vascular cast, the microanatomy of vessels being derived from the pulmonary artery was visualized with micro computed tomography. Flat-panel volumetric computed tomography provided longitudinal visualization of tissue bridges between the growing tumor and the pulmonary vasculature. In this model of peripheral parenchymal malignancy, new imaging techniques allowed effective visualization of lung tumor growth and vascularization in living mice, demonstrating a pulmonary blood supply for lung tumors. *(Am J Pathol 2005, 167:937–946)*

Lung cancer is among the most commonly occurring malignancies in the world and is one of the few that continues to show an increasing incidence.[1] Analysis of the angio-architecture of lung tumors is necessary to identify the nutritive supplier of tumor cells and to improve the efficacy of cancer therapies. In most mammals studied, the arterial vascularization of the lung is organized in two systems: a functional part from the pulmonary arteries, and nutritive vessels from the bronchial arteries, the vasa-privata of the lung.[2–4] In the adult human lung, the pulmonary arteries run alongside the airways, branching with them, and decreasing in diameter. Pulmonary vessels originate from the conus arteriosus of the right ventricle and distribute blood to the capillary bed of the alveolar sac, enabling the gas exchange.[2] In addition, the lung is supplied with systemic blood flow for nourishment by the bronchial circulation, which originates from the descending aorta and supplies the wall of the airways down to the level of the respiratory region and the vasa vasorum of the large vessels.[2–5] The origin and distribution of the bronchial vasculature varies to a large extent between and among the species.[4,6–8] However, in mouse the right bronchial artery originates from the mammaria interna and runs downwards on the right side of the trachea. On its way to the lung, it gives off branches to the trachea, esophagus, and paratracheal and mediastinal tissue. At the back of the right main brochus, it ramifies for the different lobes of the lung. Although, the left bronchial artery was small and had variable origin, which derived from the internal thoracic artery with similar branch structure as the right bronchial artery.[8,9] At the level of the terminal bronchioles, the bronchial vasculature often forms anastomoses with the pulmonary vasculature.[2]

Accepted for publication June 28, 2005.

Address reprint requests to Frank Rose, M.D., University of Giessen Lung Center, Justus Liebig University, Klinikstrasse 36, D-35392 Giessen, Germany. E-mail: Rosef@med.uni-marburg.de.

Notably, the two lung vessel types show different pathophysiological responses, namely in hypoxia and hyperoxia,[10,11] cor pulmonale,[12] fibrosis,[13] pulmonary hypertension,[14] and cancer.[7,15,16] The origin and distribution of blood supply to lung carcinomas also varies depending on the type (primary or metastatic) and stage of the tumor, and can develop from either the pulmonary or bronchial circulation or both.[6,7,15,16] To fulfill the metabolic demands of the cancer at the very early stages of its development, the pre-existing vasculature of the host supplies oxygen and nutrients. At later stages, for tumors beyond 2 to 3 mm^3, neovascularization from pre-existing vessels is necessary.[17,18]

Studies in human and animal models provide evidence that the bronchial circulation is the principle source of new vessel growth in primary lung tumors,[7,8,14,16] whereas the pre-existing pulmonary circulation has limited capacity for angiogenesis.[6] In contrast, data from metastatic lung tumors in human and animal models suggest that lung tumor perfusion originates mainly from the pulmonary circulation rather than from the bronchial circulation.[7,15,16] However, in almost one-third of the metastatic tumors, both the bronchial and the pulmonary circulation appear to participate.[7,15,16] This process might be due to new arterial anastomoses formed between the bronchial and pulmonary circulation, thus allowing the pulmonary circulation to supply nutrient flow to the tumor.[7]

The contribution of bronchial circulation to the blood supply to the lung tumors in mice is not yet understood. In the present study, we provide data that support the relevance of blood supply derived from the bronchial arteries in normal mouse lung. The main focus of the study was, however, the detailed analysis of blood supply of a primary lung tumor model [Lewis lung carcinoma cell line (LLC1)] in C57BL/6 mice. To this end, blood flow to the tumor-bearing lungs of these animals was evaluated using three different technologies: microscopic analysis of flow distribution of fluorescent microspheres, three-dimensional-reconstructed imaging by micro computed tomography (μCT) and flat-panel volumetric computed tomography (fpvCT).

Materials and Methods

Cell Culture

The C57BL/6-derived Lewis lung carcinoma cell line (LLC1) was obtained from American Type Culture Collection (Manassas, VA). The cells were routinely cultured in tissue culture flasks containing RPMI 1640 medium (PAN biotech GmbH, Aidenbach, Germany) supplemented with 2% fetal bovine serum (Greiner BioOne, Frickenhausen, Germany), penicillin (100 U/ml), and streptomycin (0.1 mg/ml) (Greiner BioOne), maintained at 37°C in humidified atmosphere containing 5% CO_2 in air.

Animals

Adult (5 to 7 weeks of age) C57BL/6 mice were purchased from Charles River, Germany, and kept under pathogen-free conditions and handled in accordance with the European Communities recommendations for experimentation.

Intratracheal Instillation

Subconfluent LLC1 cells were treated with trypsin and ethylenediamine tetraacetic acid (Gibco, Karlsruhe, Germany) and resuspended in saline. For intratracheal instillation of cells, mice were anesthetized by intraperitoneal injection of a mixture containing ketamine (Ketavet 100 mg/ml; Pharmacia & Upjohn, Erlangen, Germany) and xylazine (Rompun 2%; Bayer, Leverkusen, Germany). Later, mice were suspended in a hanging position by a rubber band fixed to the incisor teeth of the upper jaw. The trachea was intubated via the oral cavity, a Vasocan Braunüle 20-gauge 1¼“ (Braun Melsungen AG, Melsungen, Germany) tube was placed in the trachea, the cells (1×10^6/0.1 ml saline) or saline were instilled into the lungs. Next, the mice were placed on a 37°C hot plate for 10 to 15 minutes to maintain temperature. Lung tumor growth was monitored and confirmed by using both fpvCT and hematoxylin and eosin (H&E) staining. For histological analysis, lung tissues were fixed in 4% formalin and embedded in paraffin. Three-μm-thick paraffin sections were stained with H&E.

Infusion of Fluorescent Microspheres

After confirmation of tumor growth with fpvCT, animals were anesthetized by intraperitoneal injection of a mixture containing ketamine (Ketavet 100 mg/ml, Pharmacia & Upjohn, Erlangen, Germany) and xylazine (Rompun 2%, Bayer AG, Leverkusen, Germany). A polyethylene catheter was positioned either in the right ventricle or left ventricle or in both ventricles, and infused with fluorescent microspheres as described to trace pulmonary and systemic blood flow.[19–21] Because diameter of the capillaries was ~4 to 9 μm, 10-μm yellow and red fluorescent microspheres (Molecular Probes, Inc., Eugene, OR) were selected and diluted to the desired concentration with saline. Certofix Mono Complete size 1 catheter (Bayer AG) was used for infusion. Yellow fluorescent microspheres (1.5×10^5) (200 μl) were introduced into the right ventricle to trace pulmonary blood flow, and systemic blood flow was monitored with 1.5×10^5 red fluorescent microspheres (200 μl), introduced into the left ventricle. After the infusion of fluorescent microspheres, the catheters were flushed with saline containing 25,000 IU/5 ml heparin sodium (Roche, Mannheim, Germany). Later the animals were divided into two groups. One set of animals was taken for histological examination and the other set for extraction and counting the number of fluorescent microspheres.

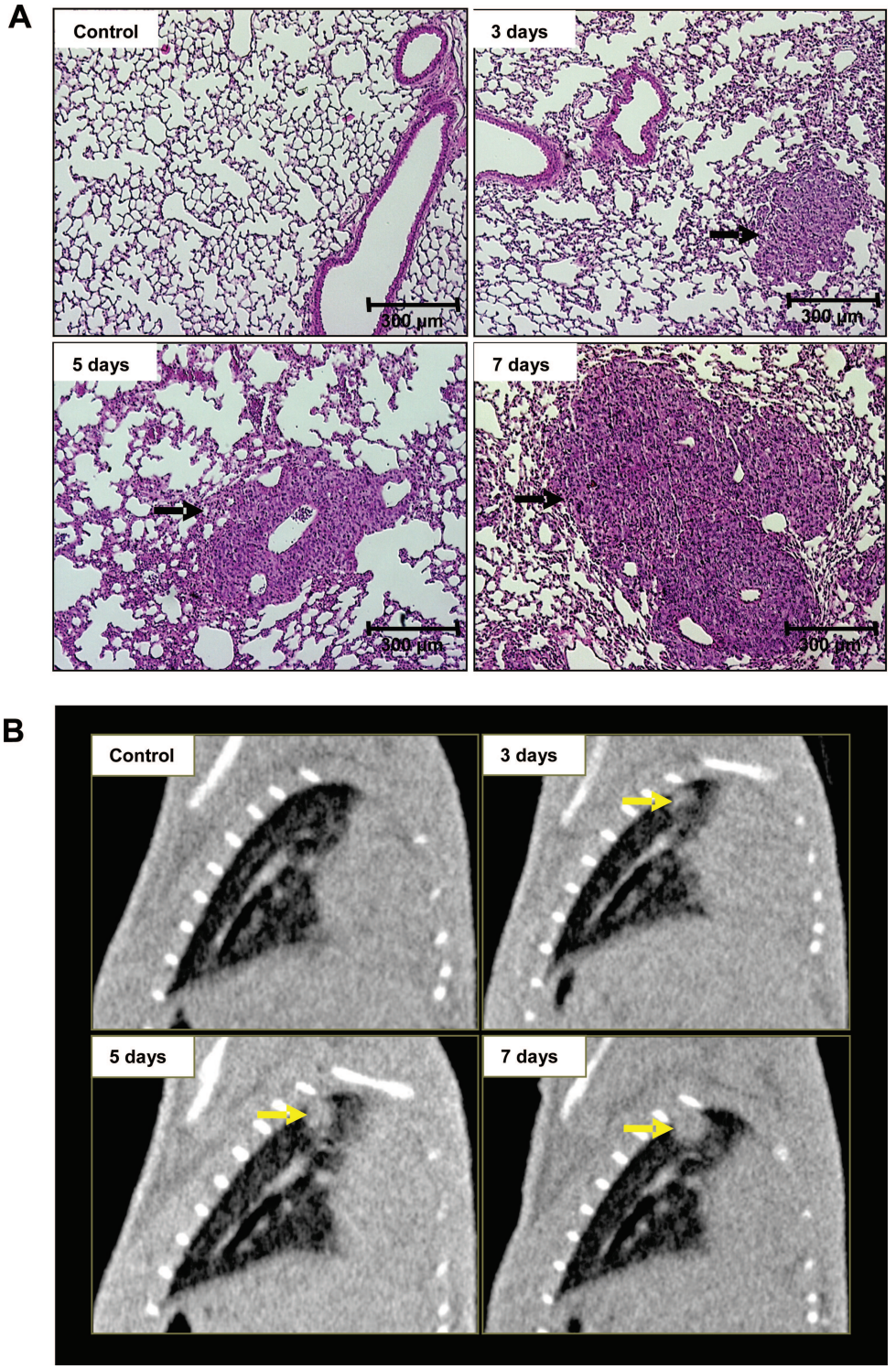

Figure 1. Analysis of lung tumor growth by histology and fpvCT. **A:** Histological analysis with H&E staining of mice lung tumor tissue sections after intratracheal instillation of saline or LLC1 cells. The cross-sections demonstrate a time-dependent increase in tumor size, with an invasive growth primarily originating from a bronchial branch (n = 6 at each time point). **B:** Tumor detection with fpvCT in C57BL/6 mice in a longitudinal study, with scanning at days 3, 5, and 7 after LLC1-tumor instillation. Representative sagittal images from independent experiments (n = 12). **Arrows** indicates tumor. Scale bars: 300 μm (**A**); 5 mm (**B**).

Histology

For cryosections, the fluorescent microsphere-infused lungs were inflated with Tissue-tek (Sakura Fine Technical Co, Ltd., Tokyo, Japan) in 0.9% NaCl (1:1). Cryosections with 15-μm slice thickness were made for histological examination using a Leica-CM 1900 cryostat microtome (Leica Instruments GmbH, Nussloch, Germany). Color and location of fluorescent microspheres within the lung and lung tumors were detected by a fluorescent microscope equipped with an IMT2RFL reflected light fluorescence attachment (Olympus Optical Co., Hamburg, Germany) multiwavelength fluorescent filter cube.[22]

Tumor and Lung Tissue Digestion and Processing

After fluorescent microsphere infusion, lungs and tumors were separated under microscopic view (Leica Instruments), their wet weights and volumes were measured and their digestion was performed as previously described.[20,21] Lungs and lung tumors were separately placed into polypropylene tubes and digested with 7 ml of a 4 mol/L KOH solution containing 0.05% Tween 80, in a water bath at 65°C until the tissue was completely dissolved. Homogenous samples were centrifuged (20 minutes, 2000 $\times$ *g*), and the supernatant was drawn off, leaving $<$1 ml behind. The remaining pellet, containing fluorescent microspheres and some debris, was rinsed with 9 ml of 0.25% Tween 80 in demineralized water at 65°C, and centrifuged again at the same force and duration. After a final rinsing with demineralized water, the pellet was resuspended in saline and analyzed for the number of fluorescent microspheres, using a hemocytometer and fluorescent microscope as described in the Fluorescent Microspheres Resource Center manual (University of Washington, Seattle, WA).[23]

Micro Computed Tomography

For investigation using μCT, blood vessels were filled with a solidifying blood-pool contrast agent (Microfil; Flow Tech, Inc., Carver, MA) forming a vascular cast. Under visual control, ready-made, nondiluted contrast was perfused manually using three different methods as described:[24–26] 1) the pulmonary vascular tree was completely filled by intravenous *in vivo* injection via the jugular vein; 2) the pulmonary arteries were successfully filled down to the capillary level by direct injection of contrast medium into the main pulmonary artery *ex vivo*; 3) the aorta and the arterial vessels were filled by injecting contrast media into a catheter inserted through left ventricle. After perfusion and solidification of the contrast medium, the lungs were removed and scanned with a desktop μCT unit (Skyscan1072; SkyScan, Aartselaar, Belgium). This system has been described in detail before.[27] In our setting, samples were positioned on a computer-controlled rotation stage and scanned over a half rotation (180°) with rotation steps of 0.675°, at 60 kVp, 100 μA. Raw data were reconstructed with a modified Feldkamp cone-beam reconstruction algorithm,[28] resulting in 8-bit gray-scale images, with 6 μm^3 isotropic voxels. Image processing and analysis were performed with the Analyze 6.0 software package (Analyze; Biomedical Imaging Resource, Mayo Foundation, Rochester, MN).

Table 1. Measurement of Tumor Growth by Histology and fpvCT

Tumor	H&E staining (diameter)	VCT (diameter)
Control	No tumor	No tumor
3 days	0.73 $\pm$ 0.10 mm	1.09 $\pm$ 0.14 mm
5 days	1.13 $\pm$ 0.12 mm	1.47 $\pm$ 0.17 mm
7 days	1.62 $\pm$ 0.08 mm	1.93 $\pm$ 0.10 mm

Measurement of tumor diameter obtained from H&E staining and fpvCT, H&E values represent the average diameter of typical tumors (n = 6, at each time points). FpvCT values represent the average diameter throughout time of a specific tumor selected in each of 12 mice, for example the tumor shown in Figure 1, A and B.

Flat-Panel Volumetric Computed Tomography

The fpvCT is a novel high-resolution CT system developed by General Electric (GE Global Research, Niskayuna, NY). In contrast to clinical CT scanners, an amorphous silicon flat-panel detector is irradiated by a cone-shaped X-ray beam. Animals were anesthetized by intraperitoneal injection of a mixture containing ketamine (Ketavet 100 mg/ml, Pharmacia & Upjohn) and xylazine (Rompun 2%, Bayer AG) and mounted on a patient table, which is moved into the gantry bore during the scan, while the X-ray tube and detector, mounted on a rotating gantry, rotate around the table. The scan is performed in a sequential rather than a helical mode. For our investigation, 120 kVp at 40 mA was used. The scanning time for one rotation was 8 seconds, covering a field-of-view of 4.2 cm in the z-direction, sufficient for scanning the thorax of one mouse. Projection images were reconstructed using a cone-beam algorithm and an edge-defining reconstruction kernel.[29,30] Data can be reconstructed at arbitrary voxel sizes, but 0.05 mm^3 isotropic voxels were used for this investigation. All data were transferred to an Advantage Windows Workstation 4.1 (GE Health Care Europe, Buc, France) and processed with the Volume Rendering software.

Results

Tumor Model

In H&E-stained histological images at 1, 3, 5, and 7 days after tumor instillation, tumor formation was noted at peripheral parenchymal region away from the airways, and the tumors increased in size from day 3 to day 7 (Figure 1A), growing from 0.73 $\pm$ 0.10 mm to 1.62 $\pm$ 0.08 mm in diameter (Table 1). Additionally, *in vivo* images obtained with fpvCT before and after instillation of LLC1 cells in the same mice (Figure 1B) detected rapid tumor development, with diameters increasing from 1.09 $\pm$ 0.14 mm at

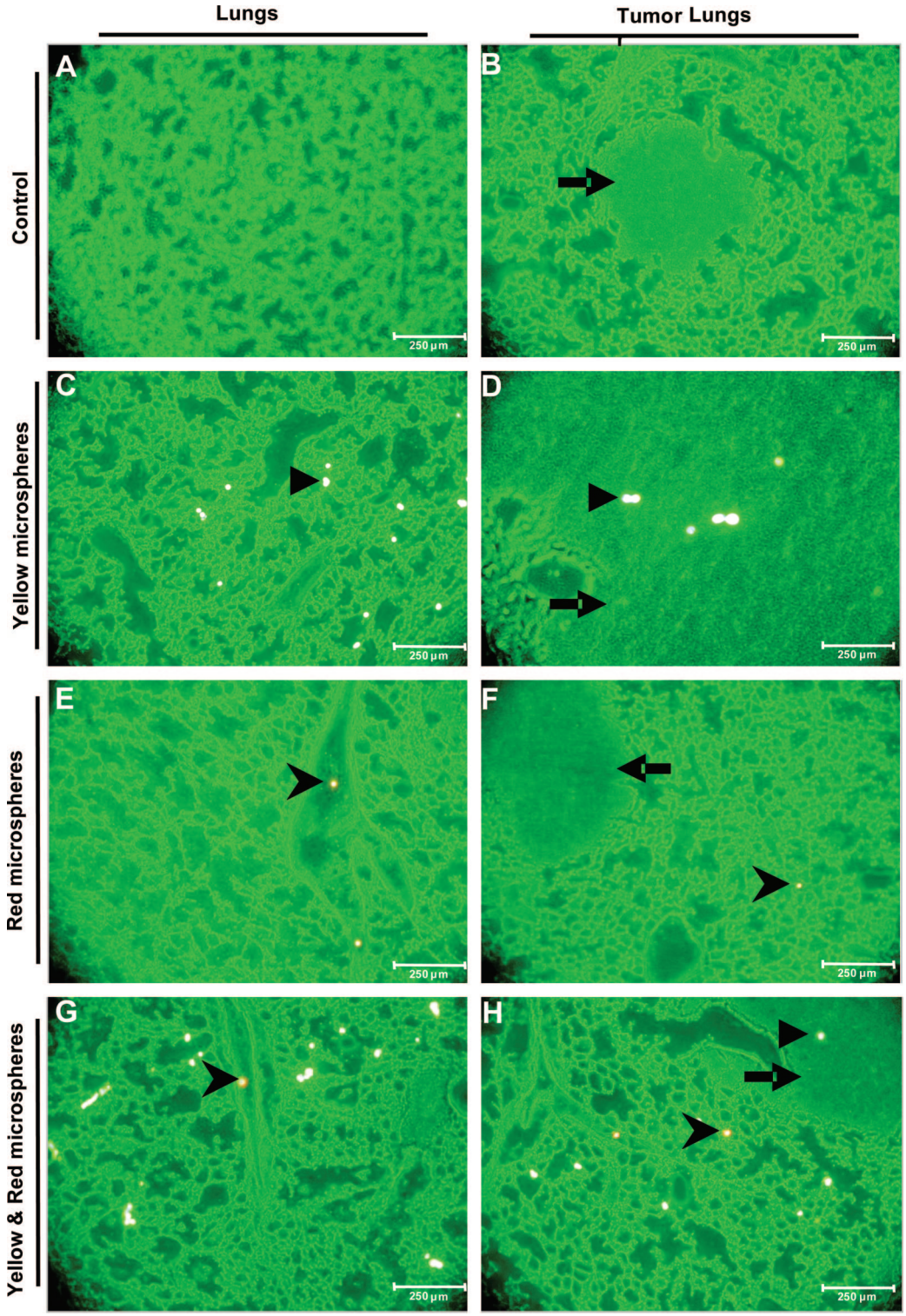

Figure 2. Blood vessel supply of healthy and tumor-bearing lung tissue analyzed by fluorescent microspheres. Cryosections of mouse lungs with (**B**, **D**, **F**, **H**) or without (**A**, **C**, **E**, **G**) tumors were analyzed with fluorescent microscopy for the presence of injected fluorescent microspheres. Lungs were fixed 7 days after LLC1 instillation when successful tumor induction was confirmed by fpvCT. The tumor lung sections show the presence of the solid tumor within the lung. Yellow fluorescent microspheres in control lung (**C**) and tumor lung (**D**), injected into the pulmonary artery, show the localization of yellow microspheres in both lung and tumor (**D**). Red fluorescent microspheres in control lung (**E**) and tumor lung (**H**), introduced via the bronchial artery, resulted in detection around the bronchial branch (**E**) or parenchyma (**F**). This observation was confirmed with simultaneous injection of both yellow and red fluorescent microspheres in control lung (**G**) and tumor lung (**H**) (n = 12). **Arrowhead** indicates yellow microspheres; **chevron** indicates red microspheres; **arrow** indicates tumor.

Table 2. Analysis of Pulmonary and Systemic Blood Flow Markers

Mouse no.	% tumor weight/ lung weight	Yellow MS/mg lung	Yellow MS/mg tumor	Red MS/mg lung	Red MS/mg tumor
1	19.86	8794.33	223.21	567.37	0.36
2	10.61	8435.75	184.21	949.72	0.53
3	20.80	9127.52	266.13	1006.71	0.32
4	9.55	9554.14	208	700.64	17.33
5	17.16	9552.24	326.08	373.13	0.43
6	19.53	8698.22	208.18	769.23	10.30
7	13.90	8609.27	267.62	794.70	0.47
8	18.32	9465.65	260.42	381.68	5.83
9	9.09	9440.55	269.23	699.30	16.92
10	18.12	9395.97	259.26	805.37	0.37
11	23.22	9225.80	243.05	903.22	0.28
12	11.56	9115.64	257.05	612.24	0.58
Average	15.98	9117.93	247.70	713.61	4.48
SEM	1.39	113.41	10.84	58.63	1.92

MS, microspheres.
Recovery of red and yellow fluorescent microspheres in the lung and lung tumors after injection of 1.5×10^5 red (left ventricle)- or yellow (right ventricle)-colored fluorescent microspheres (mean + SEM, $n = 12$).

day 3 to 1.93 ± 0.10 mm at day 7, measured in reformatted images (Table 1).

Fluorescent Microspheres in LLC1 Tumor Lungs

Microscopic images of normal lungs revealed the presence of yellow microspheres, which originated from the pulmonary artery, throughout the parenchyma (Figure 2C) and the presence of red microspheres, from the bronchial artery, close to terminal bronchi and the parenchyma (Figure 2, E and G). The parenchymal presence of microspheres from the bronchial artery might be explained by arterial anastomoses between the bronchial and pulmonary circulation and precapillary bronchial pulmonary connections of C57BL/6 mouse lung. Furthermore, microscopic images of both normal and tumor lung cryosections revealed predominance of yellow microspheres in both lung tissue and tumor tissue (Figure 2, C and D). In contrast, red microspheres were almost exclusively found in the lung tissue, with a predominant location adjacent to the bronchi (Figure 2, E and F). The absence of red microspheres in tumors indicates that virtually no perfusion of the tumor occurred via the systemic circulation. This observation was further confirmed in lung sections from mice that had microspheres introduced into both systems simultaneously (Figure 2, G and H).

In addition, the microspheres lodged in lung and tumor preparations were counted under fluorescent microscopy (Table 2). The number of yellow microspheres (supplied by the pulmonary system) was 9117 (±113) per mg of lung weight and 247 (±10) per mg of tumor weight, indicating that the tumor is less perfused than the healthy lung parenchyma (Table 2). However, a linear correlation between pulmonary vascular supply and the wet weight of the tumor was noted (Figure 3).

The number of red microspheres (supplied by the bronchial system) was 713 (±58) per mg of lung weight and 4.5 (±1.9) per mg of tumor weight, (Table 2). Furthermore, analysis of the relative vascular supply revealed an average ratio of pulmonary to systemic microspheres of 52:1 (± 0.0084) (tumor) and 13:1 (± 0.0069) (lung), a fourfold greater ratio, which confirms that the pulmonary arteries are the major feeding vessels to the tumor vasculature.

Analysis of Micro Computed Tomography Images

To identify the source of tumor vascularization, the lung vasculature was filled in three ways as described in Materials and Methods. Intravenous injection of contrast medium via the jugular vein resulted in complete fixation of the pulmonary vascular tree with preservation of microarchitecture and three-dimensional interconnectivity. In comparison *ex vivo* administration of contrast medium via the pulmonary artery resulted in successful filling of the pulmonary arteries down to the capillary levels. Both filling methods provided a clear visualization of pulmonary artery branching to LLC1 lung tumors. The third

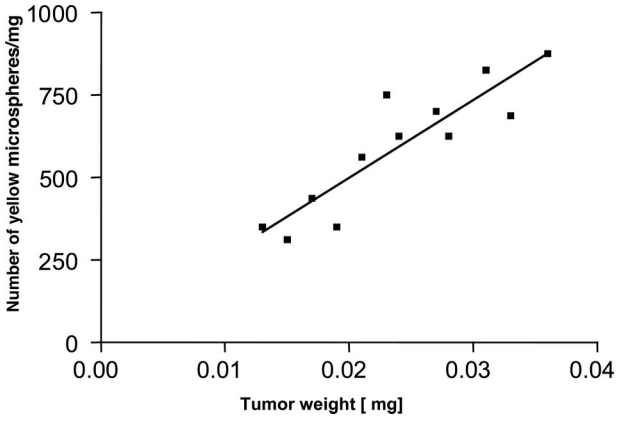

Figure 3. Correlation of blood flow to tumor weight of LLC1 lung tumors. Blood flow (indicated by number of yellow microspheres) in LLC1 tumors after 1 week correlates linearly with tumor weight (in mg) ($r^2 = 0.8$, $P < 0.0001$, $n = 12$).

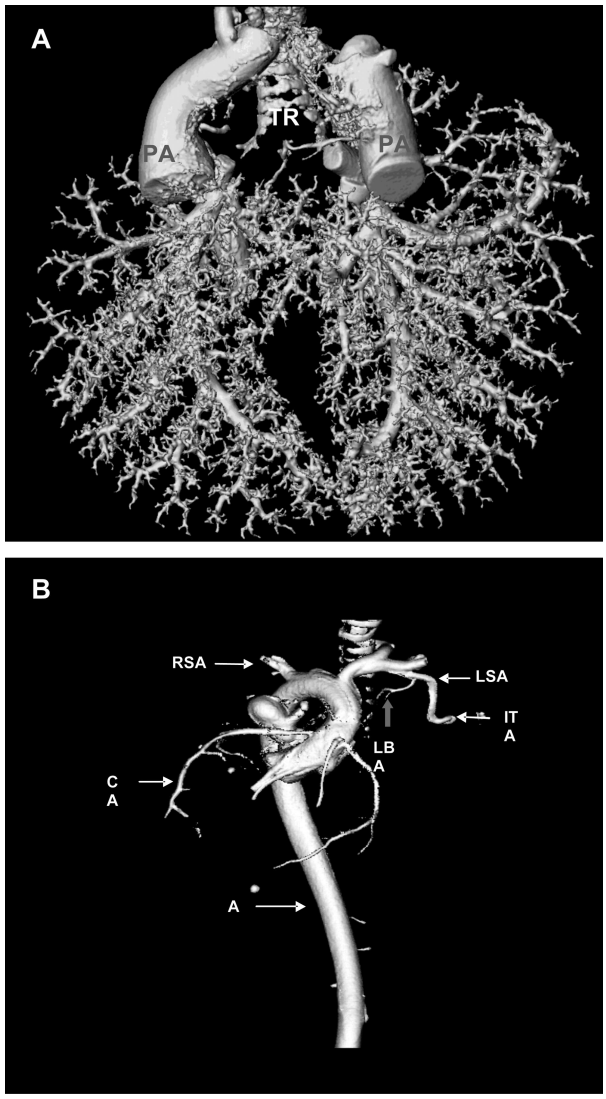

Figure 4. VRT images of the μCT. **A:** Three-dimensional VRT image of the contrast fluid-filled pulmonary artery showed branching and distribution of the pulmonary artery (PA) throughout the whole lung. **B:** Three-dimensional VRT image of the contrast fluid-filled aorta showed systemic arteries and indicates the main anatomical features such as the origin, branches, and topography of the aorta (AO), including the left bronchial artery (LBA) branching from the left subclavian artery (LSA). In addition, the presence of right subclavian artery (RSA), internal thoracic artery (ITA), and coronary artery (CA) were also demonstrated ($n = 12$).

filling approach, administration of contrast medium via the aorta demonstrated the origin of the bronchial artery at the level of main stem bronchi branching from the subclavian artery, in addition to the negligible role of bronchial arteries to LLC1 lung tumors.

For two- or three-dimensional presentations of intrapulmonary tumors and their vascularization μCT images were reconstructed using three-dimensional maximum intensity projection (MIP), three-dimensional volume-rendering technique (VRT) and two-dimensional multiplanar reconstructions (MPR). The three-dimensional VRT μCT images (Figure 4, A and B) of contrast medium-filled lungs clearly showed branching and distribution of the pulmonary artery throughout the whole lung (Figure 4A). The origin of the bronchial artery at the level of main stem bronchi branching from the subclavian artery was also visualized (Figure 4B).

Three-dimensional MIP μCT image of contrast medium-filled lungs displayed fewer large and small pulmonary vessels and their draining into tumors (Figure 5A). In addition, coronal two-dimensional MPR serial images of the tumor lungs showed the entry and branching of the pulmonary artery in the LLC1 tumor mass (Figure 5B), which is demonstrated more clearly on the magnification MIP image view (Figure 5C). All vascular filling approaches displayed branching of small pulmonary vessels inside the tumors without the existence of bronchial arterial branching. This observation from μCT scanning confirms the results obtained with the fluorescent microspheres, confirming that the pulmonary artery is the predominant tumor blood supplier.

Repetitive Analysis of fpvCT Images in Living Mice

To obtain detailed characterization of Lewis lung carcinoma mice model *in vivo*, noninvasive high-resolution fpvCT was used. The scanning revealed close attachment of the lung tumors to the pulmonary artery. Small tissue bridges suggest tumor nutrition from branches of the attached vessels (Figure 6; A to D). Both pulmonary arteries and veins are connected to the tumor by such bridges. This observation confirms primary nutrition of the tumor from the pulmonary circulation. The fpvCT permitted tumor detection down to a size of ~0.1 mm.

Discussion

This study describes for the first time, the blood flow distribution to LLC1 lung tumors in an experimental C57BL/6 mouse model. Using the combination of fluorescent microsphere infusions and subsequent microscopic analysis, and three-dimensional images obtained by μCT and fpvCT, we identified the pulmonary artery as the major source of blood supply to the tumor vasculature in this orthotopic model of lung cancer. Based on previous observations in nude mice, in which the diameter of the capillaries was measured as 4 to 9 μm,[23,31] 10-μm microspheres with different fluorescent colors were used in our experiments. Our data revealed an average ratio of microspheres originating from the pulmonary to systemic systems as 13:1 (lung) and 52:1 (tumor). These data support the known fact that pulmonary arteries are the major feeding vessels of the lung parenchyma. Interestingly, the predominance of the pulmonary over systemic blood supply was further increased (fourfold) for the LLC1 lung tumor tissue.

The microvasculature of lung tumors was also analyzed by μCT and fpvCT techniques in a follow-up study up to 1 week after tumor cell seeding. μCT is a high-resolution imaging technique for detailed analysis of complex micro architecture within organs, allowing the entire lung to be studied intact, without physically sectioning or disrupting the tissue.[27,28] It does, however,

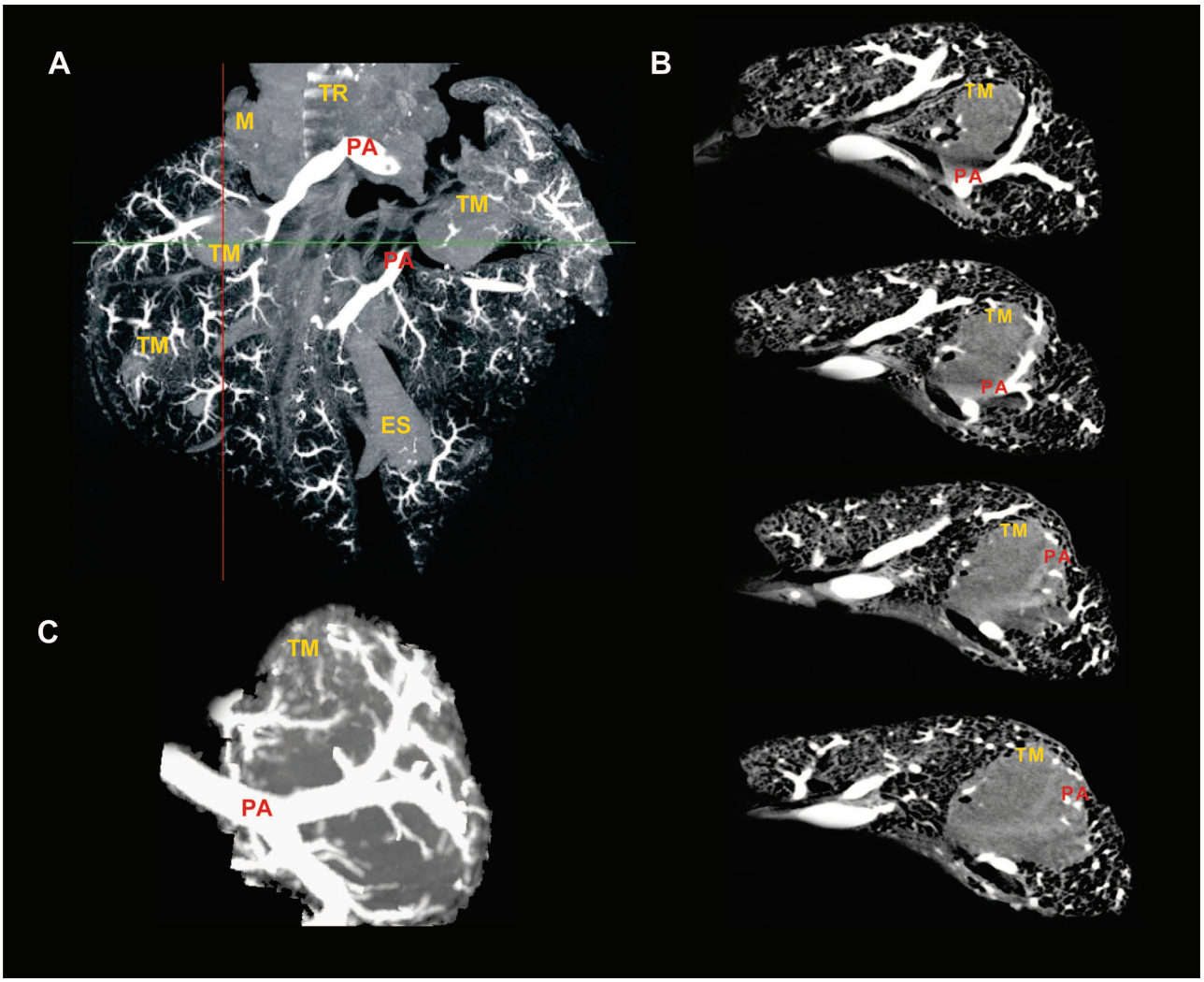

Figure 5. MIP and MPR images of the μCT. **A:** Three-dimensional MIP image of the contrast fluid-filled pulmonary artery showed branching and distribution of the pulmonary artery (PA) through the tumor mass (TM). In addition, the main anatomical features such as trachea (TR), mediasternum (M), and esophagus (ES) were also visualized. **B:** Coronal two-dimensional MPR images of the tumor lung showed the pulmonary artery (PA) passing through the LLC1 lung tumor mass (TM). Magnification of three-dimensional MIP image showed the increase of pulmonary artery (PA) vessel density around the tumor mass (TM) and visualizes vessels infiltrating the tumor (**C**) (n = 12).

require filling the vessels of interest with a vasculature cast, therefore this is exclusively an *ex vivo* method. Three-dimensional reconstructed images obtained by μCT revealed the entry and branching of the pulmonary artery in lung tumors, and detected capillaries down to 9 μm in diameter. In addition, three-dimensional images of the contrast medium-filled aorta illustrated the origin of the bronchial artery branching from the subclavian artery. This finding agrees with the observations of Verloop[9] who studied the systemic blood vessels to the lung by using casting material.

In agreement with the μCT data, three-dimensional fpvCT images also revealed close attachment of the lung tumors to the pulmonary artery. FpvCT allows volumetric visualization of small pulmonary tumors down to a diameter of ~200 μm, and is a valuable tool for estimating tumor growth of relatively small lesions within reasonably short scan intervals. Notably, this technique may be used for longitudinal *in vivo* studies. The three-dimensional images obtained by fpvCT confirm not only the location of the tumors close to the pulmonary arteries, but also documented tissue bridges connecting pulmonary vasculature to the nodules. Although no contrast medium was applied in this investigation, tumor nutrition by the pulmonary circulation can be confirmed. Noninvasive fpvCT revealed high sensitivity in tumor detection and therefore proved to be a useful tool in lung tumor screening in this orthotopic tumor model. This technique enables longitudinal studies of tumor growth and tumor response to therapy in a single animal. Therefore, sacrificing a large number of animals is not required.

In almost all types of cancer, tumor cells grow into solid neoplasm by using the host's pre-existing vasculature. In the lung, vessels may originate from the pulmonary or bronchial systems, or both. Earlier studies that used animal models to probe the origin of vascularization in the process of lung tumor growth reported conflicting results. Predominant nutrient supply was observed from both the

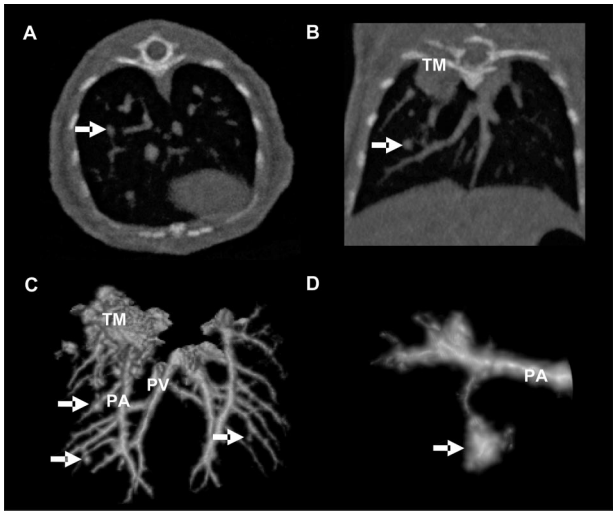

Figure 6. *In vivo* fpvCT scanning of LLC1 lung tumors. Documentation of a lung nodule (0.5 mm in diameter, **arrow**) in axial (**A**) and coronal (**B**) projections imaged with fpvCT. The voxel size was 0.05 mm in an isotropic dataset. Therefore, three-dimensional visualization was easily available. **C:** Surface rendering of the pulmonary arteries (PA) and pulmonary veins (PV) with the adjacent nodules (**arrow**) as well as a large tumor mass (TM) in the apical lobe of the right lung. **D:** Magnification of the nodule displayed in the reformatted slices (**A**, **B**) shows the soft-tissue bridge from tumor to the adjacent pulmonary artery ($n = 12$) (**arrow** indicates lung nodule).

pulmonary and bronchial systems, via enlarged bronchial vessels.[6,7,14–16,23]

These discrepancies might in part be explained by the tumor stage,[7] the species, the tumor origin (primary tumor, metastasis), and the distribution (central, peripheral) of lung neoplasms. Milne and Zerhouni[15] demonstrated the predominant perfusion of metastatic lung tumors by the pulmonary circulation in humans and rats. In contrast, Muller and Meyer-Schwickerath[7] emphasized the prime role of bronchial arteries in the vascularization of bronchogenic carcinoma at different stages of its development using postmortem angiographic and histological investigation. This process might also include new arterial anastomoses formed between the bronchial and pulmonary circulation.[6,7,15] In primary lung tumors, studies using *in vivo* angiography by Jonas and Carrington[16] suggested the bronchial arterial supply to be the primary source of nourishment in dogs. To the best of our knowledge, vascular supply of lung tumors in mice has not previously been investigated.

In a model of pulmonary blood flow obstruction in C57BL/6 mouse lung, Mitzner and colleagues[6] demonstrated the origin of neovascularization from systemic intercostal arteries and the absence of a functional bronchial circulation at the level of intraparenchymal airways. In that study, neovascularization was provoked by predominant obstruction of 40% of the pulmonary circulation. In our study, in contrast, the blood supply of primary tumors by smaller vessels and capillaries was investigated. These vessels ensure the nutrition of the tumor in a self-adjusting process, involving the liberation of growth factors, hormones, and cytokines.

Our conclusion that bronchogenic blood supply of lung parenchyma and tumor tissue is existent in C57BL/6 mice is based on 1) the presence of bronchogenic blood flow markers in both healthy lungs and LLC1 tumors; 2) the detection of fluorescent microspheres in the cryosections; 3) the three-dimensional reconstruction of μCT images, which clearly demonstrate a left bronchial artery at the level of the main stem bronchi originating from the subclavian artery, which is consistent with studies in different species;[6–8,14,16] 4) the possibility of arterial anastomoses between the bronchial and pulmonary circulation, precapillary bronchial pulmonary connections, or the tumor-associated arteriovenous malformations, through which microspheres could traverse the lungs without being trapped by capillaries, as suggested by our observation of systemically applied (red) microspheres, found in the parenchymal capillaries of the lung (Table 2, Figure 2H).

In conclusion, this study demonstrates that although the bronchogenic blood supply exists in C57BL/6 mice, the pulmonary arterial system plays the predominant role for the blood supply of LLC1 lung tumors in this species, based on analysis of fluorescent microsphere distribution and by CT imaging techniques. These findings thereby well reason the successful growth of lung carcinomas in a rather hypoxic environment. We remark the value of the experimental model of primary lung tumors induced by LLC1 cells in the mouse lung. This is the first experimental model performed in mouse. It has important implications for understanding the tumor pathophysiology and its vascular microanatomy. These findings can be applied for identifying novel targets for anticancer treatment and for site-specific drug targeting.

Acknowledgments

We thank Paul Fitzgerald (General Electric Global Research, Niskayuna, NY) and Leigh Marsh for careful proofreading of the manuscript.

References

1. Jemal A, Murray T, Samuels A, Ghafoor A, Ward E, Thun MJ: Cancer statistics 2003. CA Cancer J Clin 2003, 53:5–26
2. Hislop AA: Airway and blood vessel interaction during lung development. J Anat 2002, 201:325–334
3. Hislop A, Reid L: Normal structure and dimensions of the pulmonary arteries in the rat. J Anat 1978, 125:71–83
4. Baile EM: The anatomy and physiology of the bronchial circulation. J Aerosol Med 1996, 9:1–6
5. ad hoc Statement Committee: American Thoracic Society. Mechanisms and limits of induced postnatal lung growth. Am J Respir Crit Care Med 2004, 170:319–343
6. Mitzner W, Lee W, Georgakopoulos D, Wagner E: Angiogenesis in the mouse lung. Am J Pathol 2000, 157:93–101
7. Muller KM, Meyer-Schwickerath M: Bronchial arteries in various stages of bronchogenic carcinoma. Pathol Res Pract 1978, 163:34–46
8. Ferreira PG, Silva AC, Águas AP, Pereira AS, Grande NR: Detailed arrangement of the bronchial arteries in the Wistar rat: a study using vascular injection and scanning electron microscopy. Eur J Anat 2001, 5:67–76
9. Verloop MC: On the arteriae bronchiales and their anastomosing with the arteria pulmonalis in some rodents; a micro-anatomical study. Acta Anat 1949, 7:1–32
10. Hislop A, Reid L: New findings in pulmonary arteries of rats with

hypoxia-induced pulmonary hypertension. Br J Exp Pathol 1976, 57:542–554
11. Roberts RJ, Weesner KM, Bucher JR: Oxygen induced alterations in lung vascular development in the newborn rats. Pediatr Res 1983, 17:638–375
12. Sadigurasky M, Andrade ZA: Pulmonary changes in schistosomal cor pulmonale. Am J Trop Med Hyg 1982, 31:774–784
13. Peao MN, Aguas AP, de Sa CM, Grande NR: Neoformation of blood vessels in association with rat lung fibrosis induced by bleomycin. Anat Rec 1994, 238:57–67
14. Ley S, Kreitner KF, Morgenstern I, Thelen M, Kauczor HU: Bronchopulmonary shunts in patients with chronic thromboembolic pulmonary hypertension: evaluation with helical CT and MR imaging. Am J Roentgenol 2002, 179:1209–1215
15. Milne EN, Zerhouni EA: Blood supply of pulmonary metastases. J Thorac Imaging 1987, 2:15–23
16. Jonas AM, Carrington CB: Vascular patterns in primary and secondary pulmonary tumors in the dog. Am J Pathol 1969, 56:79–95
17. Shijubo N, Kojima H, Nagata M, Ohchi T, Suzuki A, Abe S, Sato N: Tumor angiogenesis of non-small cell lung cancer. Microsc Res Tech 2003, 60:186–198
18. Yano S, Nishioka Y, Goto H, Sone S: Molecular mechanisms of angiogenesis in non-small cell lung cancer, and therapeutics targeting related molecules. Cancer Sci 2003, 94:479–485
19. Wu CH, Lindsey DC, Traber DL, Cross CE, Herndon DN, Kramer GC: Measurement of bronchial blood flow with radioactive microspheres in awake sheep. J Appl Physiol 1988, 65:1131–1139
20. Iwamaru A, Watanabe M, Yu S, Ohtsuka T, Horinouchi H, Kobayashi K: Measurement of tumor blood flow using colored dye extraction microspheres in two rat tumor models. Int J Oncol 2001, 18:227–232
21. Iwamaru A, Watanabe M, Ohtsuka T, Horinouchi H, Kobayashi K: Analysis of angiogenic profiles by estimation of tumor blood flow with colored dye extraction microspheres after antiangiogenic therapy. Oncol Rep 2003, 10:1127–1131
22. Wagner EM, Brown RH: Blood flow distribution within the airway wall. J Appl Physiol 2002, 92:1964–1969
23. Bernard SL, Glenny RW, Polissar NL, Luchtel DL, Lakshminarayan S: Distribution of pulmonary and bronchial blood supply to airways measured by fluorescent microspheres. J Appl Physiol 1996, 80:430–436
24. Kwon HM, Sangiorgi G, Ritman EL, Lerman A, McKenna C, Virmani R, Edwards WD, Holmes DR, Schwartz RS: Adventitial vasa vasorum in balloon-injured coronary arteries: visualization and quantitation by a microscopic three-dimensional computed tomography technique. J Am Coll Cardiol 1998, 32:2072–2079
25. Kantor B, Ritman EL, Holmes Jr DR, Schwartz RS: Imaging angiogenesis with three-dimensional microscopic computed tomography. Curr Interv Cardiol Rep 2000, 3:204–212
26. Jorgensen SM, Demirkaya O, Ritman EL: Three-dimensional imaging of vasculature and parenchyma in intact rodent organs with X-ray micro-CT. Am J Physiol 1998, 275:H1103–H1114
27. Langheinrich AC, Bohle RM, Greschus S, Hackstein N, Walker G, Gerlach S, Rau WS, Hoelschermann H: Artherosclerotic lesions at micro CT: feasibility for analysis of coronary artery wall in autopsy specimens. Radiology 2004, 231:675–681
28. Feldkamp LA, Goldstein SA, Parfitt AM, Jesion G, Kleerekoper M: The direct examination of three-dimensional bone architecture in vitro by computed tomography. J Bone Miner Res 1989, 4:3–11
29. Kiessling F, Greschus S, Lichy MP, Bock M, Fink C, Vosseler S, Moll J, Mueller MM, Fusenig NE, Traupe H, Semmler W: Volumetric computed tomography (vct): a novel technology for non-invasive high resolution monitoring of tumor angiogenesis. Nat Med 2004, 10:1133–1138
30. Kalender WA: The use of flat-panel detectors for CT imaging. Radiologe 2003, 43:379–387
31. Lehr HA, Leunig M, Menger MD, Nolte D, Messmer K: Dorsal skinfold chamber technique for intravital microscopy in nude mice. Am J Pathol 1993, 143:1055–1062